JACS
JOURNAL OF THE AMERICAN CHEMICAL SOCIETY

ARTICLE

pubs.acs.org/JACS

Structural, Optical, and Electronic Properties of a Series of 3,4-Propylenedioxythiophene Oligomers in Neutral and Various Oxidation States

Chuanwen Lin, Takanori Endo, Masayoshi Takase, Masahiko Iyoda, and Tohru Nishinaga*

Department of Chemistry, Graduate School of Science and Engineering, Tokyo Metropolitan University, Hachioji, Tokyo 192-0397, Japan

Supporting Information

ABSTRACT: A series of 3,4-propylenedioxythiophene (ProDOT) oligomers ($n\mathbf{P}_{\mathbf{Hex}}$) with dihexyl side chains and methylthio end-capping units was synthesized as a model of poly(3,4-alkylenedioxythiophene)s. The slope of the linear relationship between the energy of the absorption maxima of $n\mathbf{P}_{\mathbf{Hex}}$ in the neutral states and the reciprocal of the number of monomer units ($1/n$) was found to be comparable to that of 3,4-ethylenedioxythiophene (EDOT) oligomers, suggesting that both the ProDOT and the EDOT oligomers have a similar effective conjugation. In cyclic voltammetry measurements, both the first and second oxidation waves and the third and fourth waves were shown to merge into one peak with increasing chain length. The stepwise chemical oxidations of $n\mathbf{P}_{\mathbf{Hex}}$ with $SbCl_5$ in CH_2Cl_2 at room temperature gave their stable cationic species in various oxidation states, and it was found that only the radical cations (polarons) have an obvious absorption band in the visible region. Interestingly, when the absorption spectra of tetramer radical cation $\mathbf{4P}_{\mathbf{Hex}}^{+\cdot}$ were measured at low temperatures, reversible disproportionation into dication $\mathbf{4P}_{\mathbf{Hex}}^{2+}$ and neutral species $\mathbf{4P}_{\mathbf{Hex}}$ was observed in addition to π-dimer formation. Furthermore, the radical cations of the longer oligomers showed only the disproportionation reaction. From the comparisons of the results of experiments and the theoretical calculations of the dications, $\mathbf{6P}_{\mathbf{Hex}}^{2+}$ was found to have a closed-shell nature, and only a weak singlet biradical character appeared even in longer oligomers $\mathbf{10P}_{\mathbf{Hex}}^{2+}$ and $\mathbf{12P}_{\mathbf{Hex}}^{2+}$. Overall, the electron-donating dioxy substituents are considered to stabilize high p-doping levels with closed-shell dication (bipolaron) structures in poly(3,4-alkylenedioxythiophene)s, which enables the transparency properties of the polymers.

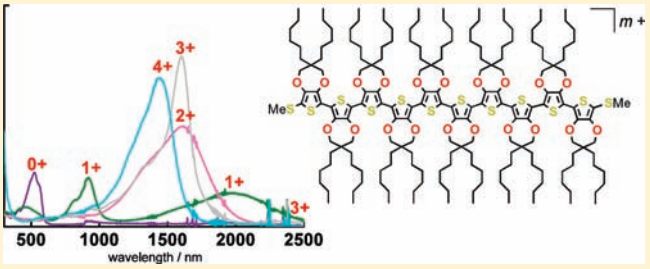

INTRODUCTION

Poly(3,4-ethylenedioxythiophene) (PEDOT) is the most successful conductive polymer.[1] PEDOT films with high conductivity (~700 S/cm) are easily accessible through in situ polymerization of 3,4-ethylenedioxythiophene (EDOT). The PEDOT complex with poly(styrene sulfonic acid) (PSS) that is dispersed in an aqueous medium is commercially available and from moderately to highly conductive PEDOT-PSS films can also be easily prepared from the water dispersion. These PEDOT films are stable under ambient conditions in the positively oxidized (p-doped) conductive states and have transparent properties. Because of these unique properties, PEDOTs are used for various applications, such as antistatic coatings, cathodes in capacitors, through-hole plating, OLED's, OFET's, photovoltaics, and electrochromic films.[1] As an analogue of PEDOT, poly(3,4-propylenedioxythiophene)s (PProDOTs) were also prepared.[2−5] One advantage in using a propylene bridge instead of an ethylene bridge is that solubilizing side chains can be introduced in a symmetrical manner when two same units are substituted at the center of the propylene bridge. The p-doped states of these polymers are also transparent, and the solution-processable electrochromic films have also been developed.[2,4]

In order to understand the unique properties of these poly(3,4-alkylenedioxythiophene)s, it is informative to study well-defined oligomers with various conjugation lengths.[6] However, despite the stability of PEDOT in p-doped states, the study of the unmodified EDOT oligomers[7] appears to be difficult, since even a trimer of EDOT has been reported to be highly unstable in neutral state.[7b] To overcome this problem, various end-capping groups, such as mesitylthio,[8] phenyl,[9,10] hexyl,[11] and trimethylsilyl[12] substituents, have been introduced onto the EDOT oligomers. Thus far, the prepared length of the oligomers has reached up to five repeated EDOT units,[12] but the limited solubility hampers the synthesis of the longer oligomers. On the other hand, ProDOT-based oligomers have received much less attention, and systematic studies on the properties of oligo-ProDOTs have not yet been reported, although the units have recently been utilized for designed molecules that act as functional materials.[13]

As in the case of EDOT oligomers,[9,10] various research groups have intensively investigated the electronic structure of cationic

Received: April 18, 2011
Published: June 16, 2011

oligothiophenes as models of p-doped conductive polythiophenes.[14−23] We also previously reported the properties of cationic species of two types of oligothiophene-based molecules. For one type, we reported on the preparation of oligothiophenes annelated with bicyclo[2.2.2]octene units. By virtue of the unusual stabilizing effect of bicyclo[2.2.2]octene annelation,[24] we succeeded in the first systematic study of the X-ray structural analyses of the radical cation salts of the dimer and the trimer and the dication salts of the tetramer and the hexamer.[25] For our second type of molecule, we prepared thiophene-pyrrole mixed oligomers end-capped with methylthio groups.[26] Combined density functional theory (DFT) calculations, UV−vis−NIR, and superconducting quantum interference device (SQUID) measurements revealed that the ground-state electronic structure of the oligomer dication composed of two pyrrole groups and six to seven thiophene rings was dominated by a singlet biradical character. In the latter system, the methylthio units were shown to play a critical role in the stabilization of the biradical dication in the longer oligomers. Otherwise, we found that the electrochemical polymerization took place during cyclic voltammetry (CV) measurements.[26]

For a detailed understanding of the electronic structure of polythiophenes at high p-doping levels, the study of longer oligothiophenes in three or more electron oxidation states is important in addition to the study of the radical cations and dications. Although several studies have mentioned the spectral observation of oligothiophene in higher electron oxidation states,[20d,f,22] little is known about their properties. In our previous systems, such studies could not be achieved due to the low solubility of these molecules in the higher oxidation states. Thus, we decided to prepare ProDOT-Hex oligomers $n\mathbf{P}_{\mathbf{Hex}}$ with dihexyl units at each propylene bridge in the hopes of enhancing their solubility and using methylthio end-capping units to protect an irreversible α-coupling upon oxidative doping. We report here on the preparation of the ProDOT-Hex oligomers up to the dodecamer. We also report the chemical generation of stable cationic species up to the hexacation, and their structural and electronic properties were investigated with electronic absorption, electron spin resonance (ESR), and NMR spectroscopy in addition to DFT calculations of the model oligomers $n\mathbf{P}_{\mathbf{H}}$. Based on these studies, we discuss the role of the dioxy substituents in the transparency properties of poly(3,4-alkylenedioxythiophene)s.

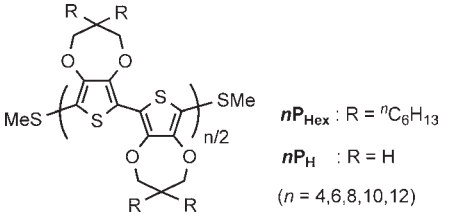

$n\mathbf{P}_{\mathbf{Hex}}$: R = ^{n}C$_6H_{13}$

$n\mathbf{P}_{\mathbf{H}}$: R = H

(n = 4,6,8,10,12)

RESULTS AND DISCUSSION

Synthesis. ProDOT-Hex monomer **1**, which consists of ProDOT and dihexyl side chains, was prepared by transetherification between 3,4-dimethoxythiophene and 2,2-dihexyl-1,3-propandiol.[4e] As shown in Scheme 1, dimerization of **1** was conducted by oxidative coupling of the lithiated monomer with Fe(acac)$_3$[4c,7c] to give ProDOT-Hex dimer **2** in good yield. In contrast to EDOT dimer,[7c] monolithiation of **2** with n-BuLi in THF proceeds smoothly, and the resulting lithiated dimer was reacted with dimethyldisulfide to give methylthio-dimer **3**. Iodination of **3** with *N*-iodosuccinimide (NIS) in THF gave iodide **4**, and Stille coupling of **4** with the stannylated ProDOT-Hex monomer and dimer gave ProDOT-Hex trimer **5** and tetramer **6** end-capped with a methylthio unit at one side. Trimer **5** and tetramer **6** were brominated with *N*-bromosuccinimide (NBS) to give the corresponding bromides **7** and **8**. Stille coupling of **7** and **8** with the stannylated ProDOT-Hex dimer gave mono methylthio-derivatives of ProDOT-Hex pentamer **9** and hexamer **10**. Finally, mono methylthio-dimer **3** was coupled via lithiation, followed by oxidation with Fe(acac)$_3$ to give $\mathbf{4P}_{\mathbf{Hex}}$, while **5**, **6**, **9**, and **10** were oxidatively coupled via radical cations using Fe(ClO$_4$)$_3$ to give $\mathbf{6P}_{\mathbf{Hex}}$, $\mathbf{8P}_{\mathbf{Hex}}$, $\mathbf{10P}_{\mathbf{Hex}}$, and $\mathbf{12P}_{\mathbf{Hex}}$, respectively.

Scheme 1. Synthesis of $n\mathbf{P}_{\mathbf{Hex}}$

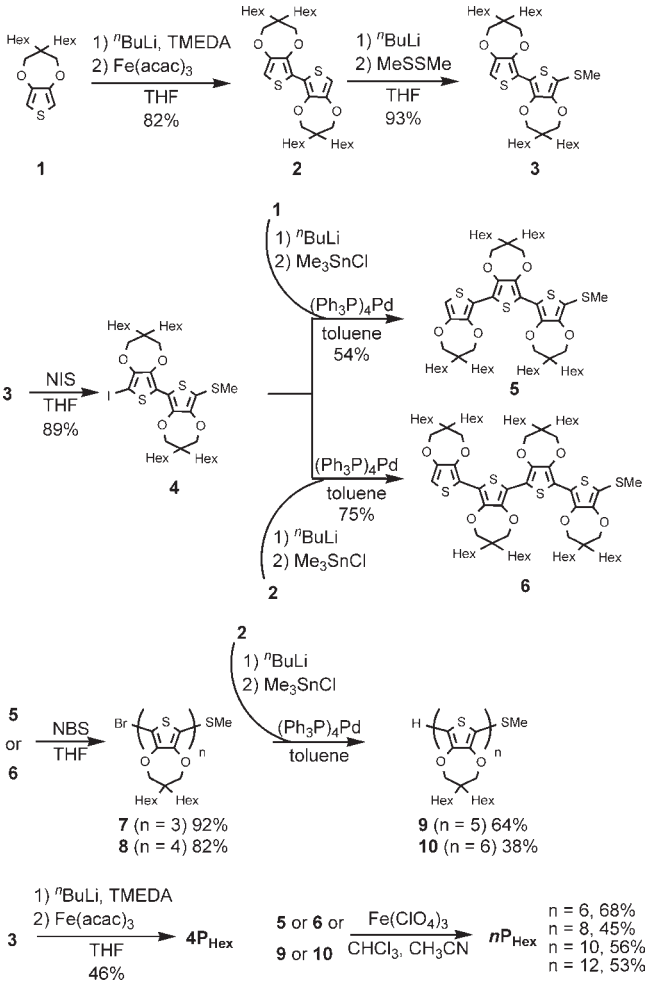

Structural and Electronic Properties in the Neutral State. During our search for an efficient synthetic route to $n\mathbf{P}_{\mathbf{Hex}}$, we prepared ProDOT-Hex dimer diiodide **11**, which was prepared by dilithiation of **2**, followed by a reaction with iodine. A single crystal of **11** was obtained from dichloromethane/hexane, and the structure was determined by X-ray crystallography. As shown in Figure 1a, the two thiophene rings of **11** adopt a coplanar conformation in the crystal, with a C═C—C═C dihedral angle of 180°. The distance between the sulfur atom of thiophene and the closer oxygen atom of the adjacent unit is 2.85 Å, which is considerably shorter than the sum of the van der Waals radii of sulfur and oxygen atoms

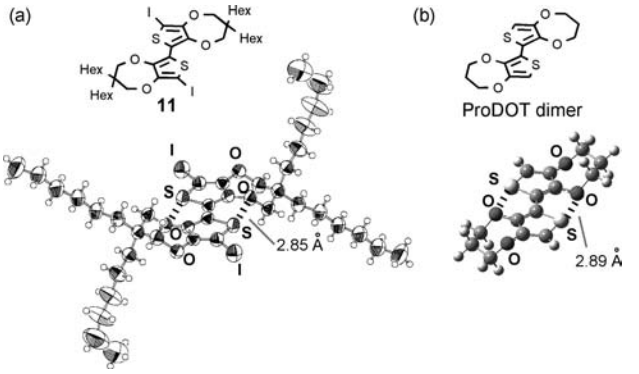

Figure 1. (a) ORTEP drawing (50% probability) showing the X-ray structure of **11** and (b) the optimized structure of ProDOT dimer at the B3LYP/6-31G(d) level.

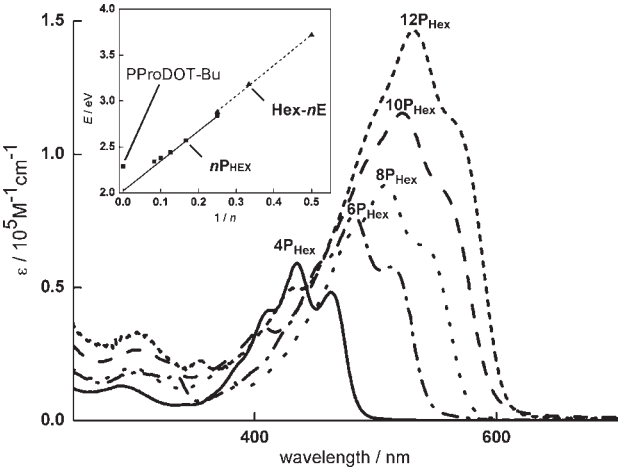

Figure 2. Absorption spectra of $n\mathbf{P}_{\mathbf{Hex}}$ in CH_2Cl_2. Plots of the energy of absorption maxima of $n\mathbf{P}_{\mathbf{Hex}}$ and **Hex-*n*E** against the reciprocal of the number of monomer units $(1/n)$ are shown in the inset.

(1.85 + 1.50 = 3.35 Å). Similar phenomena were also observed in ProDOT-Et dimer[4c] and in EDOT-containing oligomers,[11,27] although the thiophene rings were slightly twisted in these X-ray structures. The planarization and the short S···O contact in ProDOT dimer were reproduced by DFT calculations at the B3LYP/6-31G(d) level (C═C—C═C dihedral angle 180°; S···O 2.89 Å), as shown in Figure 1b. Bonding interactions between the S and O atoms were found in the highest occupied molecular orbital (HOMO)−2 and HOMO−5 (Figure S1, Supporting Information). However, the stabilization energy of the S···O interaction would be quite small, as demonstrated in the theoretical study of EDOT dimer, where no additional rotational barrier was observed.[28]

The absorption spectra of neutral $n\mathbf{P}_{\mathbf{Hex}}$ in dichloromethane at room temperature are shown in Figure 2. The shorter oligomers, $\mathbf{4P}_{\mathbf{Hex}}$ and $\mathbf{6P}_{\mathbf{Hex}}$, show a vibrational fine structure that is similar to that in the absorption spectra of the EDOT oligomers.[9,11,12] These results suggest the same rigidification by the attractive S···O interaction that is seen in the EDOT oligomers[9,11,12] also operates in the shorter ProDOT oligomers in the solution phase. However, as the chain length elongates, the fine structure of $n\mathbf{P}_{\mathbf{Hex}}$ broadens, probably due to the decreasing total rigidity of the π-system. Most oligothiophenes do not show such a fine structure in solution as that observed in the shorter EDOT and ProDOT oligomers, but these phenomena are not unique to 3,4-dioxythiophene oligomers. In the absorption spectra of a series of oligothiophenes covered with *tert*-butyldiphenylsilyl (TBDPS) groups, an analogous fine structure in shorter oligomers, and a broadening with increasing chain length were also observed.[20f] This could be accounted for by the steric repulsion between the bulky TBDPS substituents that rigidify the π-system.

Plots of the energy of the absorption maxima (E_{0+}) of $n\mathbf{P}_{\mathbf{Hex}}$ and the EDOT oligomers (n = 2−4) end-capped with dihexyl groups (**Hex-*n*E**)[11] against the reciprocal of the number of monomer units $(1/n)$ are shown in Figure 2 (inset). For $n\mathbf{P}_{\mathbf{Hex}}$, the best linear fit ($R^2$ = 0.999) was obtained only in a short oligomeric range (n = 4, 6, and 8). The linear equations for $n\mathbf{P}_{\mathbf{Hex}}$ (eq 1) and for **Hex-*n*E** (R^2 = 0.999) (eq 2) are as follows:

$$E_{0+}(\text{eV}) = 2.04 + 3.21/n \quad (1)$$

$$E_{0+}(\text{eV}) = 2.05 + 3.35/n \quad (2)$$

The slope of the plot is considered to reflect the effective conjugation.[29,30] As such, the comparable slopes of these linear regressions indicate that both the EDOT and the ProDOT oligomers have a similar effective conjugation with similar planarity. The slopes are larger than that of regioregular oligo(3-octylthiophene)s (3.15)[29] but smaller than those of unsubstituted oligothiophene (3.76).[30] These results suggest that the planarity of the ProDOT and the EDOT oligomers is higher than that of regioregular oligo(3-octylthiophene)s but is lower than that of unsubstituted oligothiophene. Therefore, it is considered that there is some steric repulsions between S···O atoms of the EDOT and the ProDOT oligomers. This repulsion would be smaller than the repulsion between the alkyl side chain and the adjacent thiophene unit in oligo(3-alkylthiophene)s but larger than that between unsubstituted thiophene rings. As described above, the calculated structures of both EDOT[28] and ProDOT dimers and the X-ray structure of **11** were shown to have a completely planar structure with a short S···O contact, whereas slightly twisted structures were observed in the X-ray structures of ProDOT-Et dimer[4c] and EDOT-containing oligomers.[11,27] Thus, the planarity of EDOT and ProDOT oligomers appears to be in a subtle balance between the attractive and repulsive S···O interactions.

The extrapolation of this type of plot is used for the prediction of the band gap of π-conjugated polymers. Recently, however, it has been pointed out that a deviation from the linear relationship occurs for longer oligomers.[31] In fact, the extrapolation of eq 1 (2.04 eV) underestimates the absorption maximum of the corresponding polymer (PProDOT-Bu in CH_2Cl_2 solution: 542 nm, 2.29 eV).[4c] For $n\mathbf{P}_{\mathbf{Hex}}$, the deviation from the linear relationship starts to occur at approximately the decamer length. In the same range, the vibrational fine structure in the absorption spectra broadens, as described above. Furthermore, recent experimental[30] and theoretical[31b] studies have demonstrated that oligothiophenes without the S···O interaction also show a similar deviation from linear relations, which starts to occur at similar oligomer lengths. Overall, the S···O interaction in the oligoProDOT does not seem especially to enhance the effective conjugation in the neutral state. Judging from the similarity between both the ProDOT and the EDOT oligomers, this conclusion would also be applicable for the EDOT oligomers.

Oxidation Potentials. The oxidation potentials of $n\mathbf{P}_{\mathbf{Hex}}$ were measured using cyclic voltammetry (CV) in CH_2Cl_2 with 0.1 M tetra-*n*-butylammonium hexafluorophosphate as the electrolyte. The voltammograms are shown in Figure 3a, and the oxidation

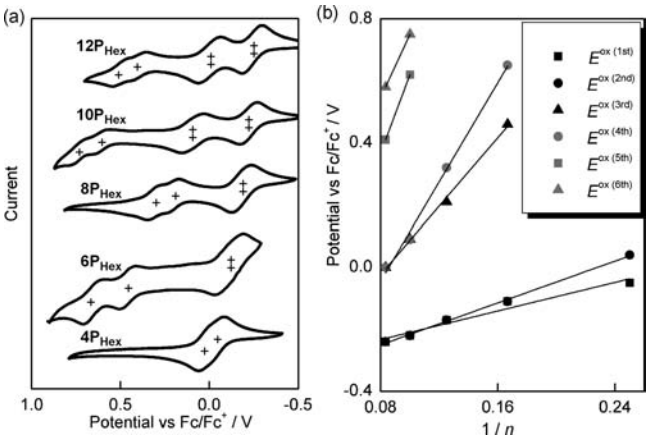

Figure 3. (a) Cyclic voltammograms of $n\mathbf{P}_{\mathbf{Hex}}$ and (b) plots of the oxidation potentials of $n\mathbf{P}_{\mathbf{Hex}}$ against the reciprocal of the number of monomer units ($1/n$).

Table 1. Oxidation Potentials (E^{ox}) of $n\mathbf{P}_{\mathbf{Hex}}$ and EDOT-Containing Oligomers MesS-2T2E, Ph-4E, and Hex-4E in CH_2Cl_2

compd	$E^{ox1}{}_{1/2}$ (V)[a]	$E^{ox2}{}_{1/2}$ (V)[a]	$E^{ox3}{}_{1/2}$ (V)[a]	$E^{ox4}{}_{1/2}$ (V)[a]
$\mathbf{4P}_{\mathbf{Hex}}$[b]	−0.05 (1e)	0.04 (1e)	–	–
$\mathbf{6P}_{\mathbf{Hex}}$[b]	−0.11 (2e)	0.46 (1e)	0.65 (1e)	–
$\mathbf{8P}_{\mathbf{Hex}}$[b]	−0.17 (2e)	0.21 (1e)	0.32 (1e)	–
$\mathbf{10P}_{\mathbf{Hex}}$[b]	−0.22 (2e)	0.09 (2e)	0.62 (1e)	0.75 (1e)
$\mathbf{12P}_{\mathbf{Hex}}$[b]	−0.24 (2e)	0.00 (2e)	0.41 (1e)	0.58 (1e)
MesS-2T2E^{in}[c,d]	0.02 (1e)	0.26 (1e)	–	–
MesS-2T2E^{out}[c,d]	0.14 (1e)	0.19 (1e)	–	–
Ph-4E[b,e]	−0.21 (1e)	−0.08 (1e)	–	–
Hex-4E[b,f]	0.22 (1e)[g]	0.61 (1e)[g]	–	–

[a] Potentials vs Fc/Fc^+, except for the data of **Hex-4E**. The "1e" and "2e" in parentheses denote one- and two-electron oxidations, respectively. [b] Concentration: 0.5 mM. Supporting electrolyte: 0.1 M Bu_4NPF_6. [c] Supporting electrolyte: 0.1 M Bu_4NBF_4. [d] ref 8. [e] ref 9. [f] ref 11. [g] Potentials vs Ag/AgCl.

potentials of $n\mathbf{P}_{\mathbf{Hex}}$ and EDOT-containing quaterthiophenes are summarized in Table 1.[8,9,11] As shown in Figure 3a, all of the oxidation steps of $n\mathbf{P}_{\mathbf{Hex}}$ were electrochemically reversible at room temperature, suggesting that multielectron oxidation states of $n\mathbf{P}_{\mathbf{Hex}}$ were stable. The first oxidation potential of tetramer $\mathbf{4P}_{\mathbf{Hex}}$ (−0.05 V vs Fc/Fc^+) is between that of the mesitylthio-end-capped quaterthiophenes which include two EDOT units at either the inside or the outside positions (**MesS-2T2E**^{in}: 0.02 V vs Fc/Fc^+, **MesS-2T2E**^{out}: 0.14 V)[8] and that of the EDOT tetramer end-capped with phenyl (**Ph-4E**: −0.21 V vs Fc/Fc^+)[9] or hexyl (**Hex-4E**: 0.22 V vs Ag/AgCl (∼ −0.2 V vs Fc/Fc^+))[11] groups. Thus, the first oxidation potential of $\mathbf{4P}_{\mathbf{Hex}}$ was as low as those of the EDOT-containing quaterthiophenes due to the electron-donating dioxy substituents, although a precise comparison is difficult due to the lesser number of dioxy-substituted thiophene rings in **MesS-2T2E** and the different type of end-capping unit in **Ph-4E** and **Hex-4E**.

The methylthio-end-capping in $n\mathbf{P}_{\mathbf{Hex}}$ caused, to some extent, a narrowing of the gap between the first and the second oxidation potentials, as observed in mesitylthio-end-capped oligothiophenes.[8,32] The gap was 0.09 V for $\mathbf{4P}_{\mathbf{Hex}}$ and became 0 V for the higher oligomers ($n \geq 6$). On the other hand, the oxidation potentials for the higher oxidation states were significantly decreased by the multiple dioxy-substituents. As a result, two-step one-electron oxidations for $\mathbf{4P}_{\mathbf{Hex}}$, one-step two-electron and two-step one-electron oxidations for $\mathbf{6P}_{\mathbf{Hex}}$ and $\mathbf{8P}_{\mathbf{Hex}}$, and two-step two-electron and two-step one-electron oxidations for $\mathbf{10P}_{\mathbf{Hex}}$ and $\mathbf{12P}_{\mathbf{Hex}}$ were observable in lower than 1.0 V vs Fc/Fc^+. Thus, for $\mathbf{10P}_{\mathbf{Hex}}$ and $\mathbf{12P}_{\mathbf{Hex}}$, even six-electron oxidations were observed as reversible steps in the potential window. Here, it is interesting to note that both the first and second oxidation peaks and the third and fourth peaks tended to merge into one peak with increasing chain length. The total six-electron oxidation, including the two-step two-electron process of $\mathbf{10P}_{\mathbf{Hex}}$ and $\mathbf{12P}_{\mathbf{Hex}}$, are in sharp contrast to the fact that sterically segregated dodecithiophenes with alkyl[20f] or aryl[33] substituents only show four-step one-electron oxidations in the same solvent and supporting electrolyte. Accordingly, for longer $n\mathbf{P}_{\mathbf{Hex}}$, the two- and four-electron oxidation states appear to be more favorable than the one- and three-electron oxidation states, whereas oligothiophenes with alkyl[20f] and aryl[33] substituents do not have such characteristics. This can be rationalized in terms of the stabilization effect of the electron-donating dioxy substituents of the ProDOT unit. We will discuss this effect further in a later section.

The chain length dependence of the redox potentials of $n\mathbf{P}_{\mathbf{Hex}}$ is summarized in Figure 3b. As observed for **Ph-***n***E**[9] and **Hex-***n***E**,[11] good linear correlations between the variation of the oxidation potentials and the reciprocal number of thiophene rings (first oxidation potentials: $R^2 = 0.958$, second: 0.998, third: 0.997, and fourth: 0.996) were observed within the oligomer length ($4 \leq n \leq 12$). The linear equations for first oxidation (eq 3), for second oxidation (eq 4), for third oxidation (eq 5), for fourth oxidation (eq 6), for fifth oxidation (eq 7), and for sixth oxidation (eq 8) potentials are as follows:

$$E^{ox(1st)}(\text{V vs Fc/Fc}^+) = -0.33 + 1.15/n \quad (3)$$

$$E^{ox(2nd)}(\text{V vs Fc/Fc}^+) = -0.38 + 1.69/n \quad (4)$$

$$E^{ox(3rd)}(\text{V vs Fc/Fc}^+) = -0.46 + 5.50/n \quad (5)$$

$$E^{ox(4th)}(\text{V vs Fc/Fc}^+) = -0.68 + 7.98/n \quad (6)$$

$$E^{ox(5th)}(\text{V vs Fc/Fc}^+) = -0.64 + 12.6/n \quad (7)$$

$$E^{ox(6th)}(\text{V vs Fc/Fc}^+) = -0.27 + 10.2/n \quad (8)$$

With the exception of the sixth oxidation potential, the slope of these linear regressions becomes steeper as the number of electrons that are oxidized per molecule increases. Similar phenomena of steeper slopes in the higher oxidation steps were also reported in diphenylamino end-capped oligothiophenes.[22] Reflecting the steeper slope, extrapolations of the oxidation potentials became more negative values in the higher oxidation steps, and hence they did not provide a common prediction for the oxidation potential for the corresponding polymers. For PProDOT-Bu, the oxidation current starts to increase at approximately −0.2 V vs Ag/Ag^{+4c} (ca. −0.3 V vs Fc/Fc^+). At this potential, the oxidation current of longer oligomers $n\mathrm{P}_{\mathrm{Hex}}$ (n = 10,12) also starts to increase. Overall, these results suggest that the similar deviation from the linear relationship, as observed in the energy of absorption maxima (vide supra), also takes place in the oxidation potential of longer oligomers.

Optical Absorptions in Various Oxidation States. To observe the optical absorption spectra in various oxidation states, chemical oxidations of $n\mathbf{P}_{\mathbf{Hex}}$ were conducted in CH_2Cl_2 by adding various amounts of $SbCl_5$ as a dilute CH_2Cl_2 solution. Each one-electron oxidation requires at least 1.5 equivalents of $SbCl_5$. As shown in Figure 4a−e, stepwise oxidations proceeding up to the dication for $\mathbf{4P}_{\mathbf{Hex}}$, the trication for $\mathbf{6P}_{\mathbf{Hex}}$, the tetracation for $\mathbf{8P}_{\mathbf{Hex}}$ and $\mathbf{10P}_{\mathbf{Hex}}$, and the hexacation for $\mathbf{12P}_{\mathbf{Hex}}$ were observed at room temperature. After reacting with an excess amount of the oxidant, it was confirmed that reduction with excess tetra-*n*-butylammonium iodide reproduced neutral $n\mathbf{P}_{\mathbf{Hex}}$. Thus, no apparent follow-up reaction occurred during the measurements. For all of the absorption bands of radical cations (marked with "1+" in Figure 4), one broad absorption band appeared in the visible region, and one broad absorption band appeared in the near-IR region. The absorptions in the visible region became very weak for all of the oligomers in more than two-electron oxidation states, with the exception of the shortest oligomer $\mathbf{4P}_{\mathbf{Hex}}$. These spectral behaviors are consistent with the transparent nature of PProDOT[4] and also PEDOT[1] in high p-doping levels.

The energies of the absorption maxima are summarized in Table 2. In the absorption spectra of radical cations (1+), the lower-energy band which can be assigned as a HOMO−singly occupied molecular orbital (SOMO) transition[21a] is as strong as the second absorption band. However, the lower-energy band for the trication (3+) was much weaker. To support the observed result, we performed time-dependent (TD) DFT calculations (UB3LYP/6-31G(d)) of the trications of $n\mathbf{P}_{\mathbf{H}}$. For the trication of the unsubstituted oligothiophene, previous theoretical calculations predicted that the doublet state is lower in energy than the quartet state.[34] Thus, the TD-DFT calculations of trications were performed in the doublet state, which well reproduced the weak oscillator strength observed in the lower-energy band (Figure S2, Supporting Information). Therefore, the weak band of trications can be assigned as a HOMO−SOMO transition of doublet radical species. Notably, similar weak absorptions at lower energies (0.55 eV) were also observed for the pentacation (5+) of $\mathbf{12P}_{\mathbf{Hex}}$.

The chain length dependence of the absorption energy of $n\mathbf{P}_{\mathbf{Hex}}$ in various oxidation states (E_{m+}) is summarized in Figure 5. As shown in the plot, good linear relations ($R^2 > 0.996$) between the energy of the absorption maxima against the reciprocal of the number of monomer units ($1/n$) were observed for all of the bands, with the exception of the lower-energy band of the monocation ($E_{1+}{}^1$: $R^2 = 0.989$) and trication ($E_{3+}{}^1$: $R^2 = 0.981$). This exception was caused by the similar saturation phenomena as those seen in the longer oligomers in the neutral state (vide supra). The linear equations for the radical cation ($E_{1+}{}^1$: eq 9, $E_{1+}{}^2$: eq 10), for the dication (E_{2+}: eq 11), for the radical trication ($E_{3+}{}^1$: eq 12, $E_{3+}{}^2$: eq 13), and for the tetracation (E_{4+}: eq 14) are as follows:

$$E_{1+}{}^1(\text{eV}) = 0.41 + 2.34/n \quad (9)$$

$$E_{1+}{}^2(\text{eV}) = 1.09 + 2.54/n \quad (10)$$

$$E_{2+}(\text{eV}) = 0.31 + 4.64/n \quad (11)$$

$$E_{3+}{}^1(\text{eV}) = 0.26 + 2.84/n \quad (12)$$

$$E_{3+}{}^2(\text{eV}) = 0.27 + 5.22/n \quad (13)$$

$$E_{4+}(\text{eV}) = 0.26 + 5.99/n \quad (14)$$

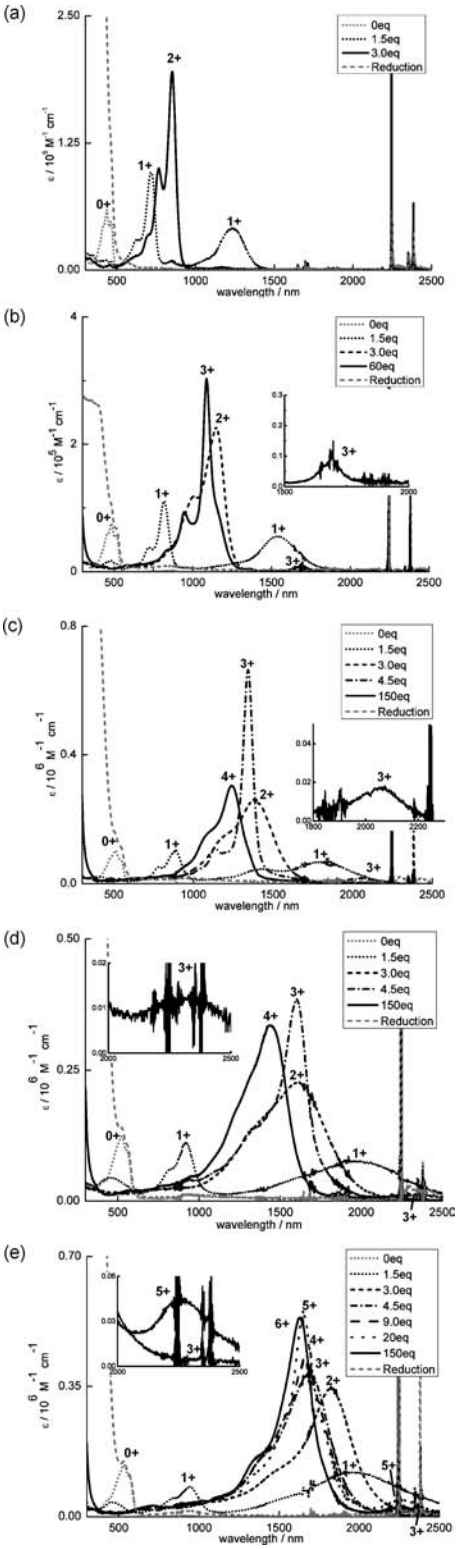

Figure 4. Absorption spectra of (a) $\mathbf{4P}_{\mathbf{Hex}}$ (33.2 μM), (b) $\mathbf{6P}_{\mathbf{Hex}}$ (50.0 μM), (c) $\mathbf{8P}_{\mathbf{Hex}}$ (16.6 μM), (d) $\mathbf{10P}_{\mathbf{Hex}}$ (17.0 μM), and (e) $\mathbf{12P}_{\mathbf{Hex}}$ (16.5 μM) in various oxidation states (1+ − 6+) obtained by adding various amounts of $SbCl_5$ in CH_2Cl_2 at room temperature. The spectra recorded after the reduction of $n\mathbf{P}_{\mathbf{Hex}}$ in its highest oxidation states with excess amounts of iodide are also shown. Insets are enlargements of the region for the lower-energy bands of the trications and pentacation.

Table 2. Energy of Absorption Maxima (E_{m+}) and Absorption Coefficients (ε) of $n\mathbf{P}_{Hex}$ in Neutral ($m = 0$) and Various Oxidation States ($m = 1-6$) in CH_2Cl_2

absorption band	$4\mathbf{P}_{Hex}$[a]	$6\mathbf{P}_{Hex}$[a]	$8\mathbf{P}_{Hex}$[a]	$10\mathbf{P}_{Hex}$[a]	$12\mathbf{P}_{Hex}$[a]
E_{0+}	2.85 (4.77)	2.57 (4.87)	2.44 (4.95)	2.38 (5.06)	2.34 (5.21)
$E_{1+}{}^1$	1.00 (4.61)	0.81 (4.75)	0.69 (4.86)	0.63 (4.88)	0.63 (5.11)
$E_{1+}{}^2$	1.73 (4.98)	1.52 (5.04)	1.40 (5.05)	1.35 (5.04)	1.31 (5.01)
E_{2+}	1.46 (5.29)	1.08 (5.35)	0.90 (5.42)	0.77 (5.36)	0.68 (5.60)
$E_{3+}{}^1$	–	0.74 (3.9)	0.60 (3.7)	0.53 (4.1)	0.51 (4.0)
$E_{3+}{}^2$	–	1.14 (5.48)	0.92 (5.82)	0.78 (5.58)	0.72 (5.62)
E_{4+}	–	–	1.00 (5.48)	0.86 (5.52)	0.75 (4.00)
$E_{5+}{}^1$	–	–	–	–	0.55 (4.65)
$E_{5+}{}^2$	–	–	–	–	0.75 (5.75)
E_{6+}	–	–	–	–	0.76 (5.72)

[a] The data of absorption energy are given in eV with log ε in parentheses.

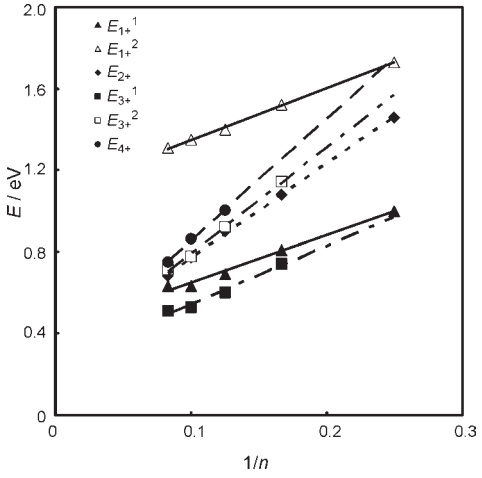

Figure 5. Plots of the energy of the absorption maxima of $n\mathbf{P}_{Hex}$ in various oxidation states against the reciprocal of the number of monomer units ($1/n$).

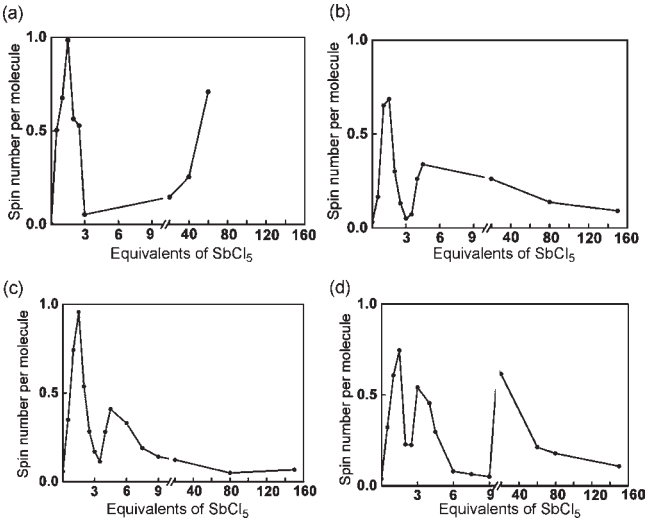

Figure 6. Changes of spin numbers of (a) $6\mathbf{P}_{Hex}$, (b) $8\mathbf{P}_{Hex}$, (c) $10\mathbf{P}_{Hex}$, and (d) $12\mathbf{P}_{Hex}$ as a function of the number of equivalents of $SbCl_5$. Spin numbers were estimated by the DPPH standard.

The transition energies of the lower-energy bands in the mono- and trications ($E_{1+}{}^1$ and $E_{3+}{}^1$) are already small, even for the shorter oligomers. Thus, the deviation from a linear relationship starts in the similar oligomeric range, as that observed in the neutral states. On the other hand, the slope becomes steeper in the higher oxidation states. In particular, the slopes for E_{2+} (4.64), $E_{3+}{}^2$ (5.22), and E_{4+} (5.99) were much steeper than that (3.21) for the neutral state. These results may reflect the greater effective conjugation for the higher oxidation states that is caused by the enhanced quinoidal character[24b] contrary to the aromatic resonance structure in the neutral state.

ESR Spectroscopy. In general, conductive polythiophenes in high p-doping levels are almost ESR-silent,[35,36] indicating that they have singlet character. At the early stage of the theoretical investigations, the singlet character was rationalized by the formation of a bipolaron[37] which, in chemical terms, corresponds to a closed shell singlet dication. To gain further insight into the origin of this singlet character, which is important for the elucidation of the nature of the charge carrier in polythiophenes, the concepts of π-dimers,[14c] σ-dimers,[38] and polaron pairs[21a] have been discussed through the study of cationic oligothiophenes. Before the detailed investigation of the corresponding species derived from $n\mathbf{P}_{Hex}$, the basic magnetic properties of $n\mathbf{P}_{Hex}$ in various oxidation states were investigated with ESR spectroscopy.

Each ESR spectra of $n\mathbf{P}_{Hex}$ in various oxidation states were measured at room temperature after checking their UV−vis−NIR spectra. A broad, one-line signal with g values of 2.0028−2.0047 (Figure S3, Supporting Information) was observed, and the spin number per molecule for $n\mathbf{P}_{Hex}$ in various oxidation states was estimated using a 1,1-diphenyl-2-picrylhydrazyl (DPPH) standard. As shown in Figure 6, the spin numbers at the one-electron oxidation level (1.5 equivalents of $SbCl_5$) reach a maximum, owing to the formation of radical cation $n\mathbf{P}_{Hex}{}^{+\bullet}$. The next oxidation level (two-electron oxidation) with a total of 3 equivalents of $SbCl_5$ resulted in the disappearance of the ESR signal, indicating that all of dications $n\mathbf{P}_{Hex}{}^{2+}$ had a singlet ground state. However, unnegligible spins were left in the longer oligomer dications, which is possibly due to the thermally excited triplet state, as observed in the relevant quinoidal oligothiophenes.[39]

As for trications $n\mathbf{P}_{Hex}{}^{3+\bullet}$, the ESR signal appears again with a spin number of less than 1 (0.3−0.7). The small spin numbers are not inconsistent with the theoretical prediction that $n\mathbf{T}^{3+}$ has doublet ground state.[34] However, these results are in contrast with the previous study on alkyl oligothiophenes, in which no apparent ESR signal was detected in more than three-electron

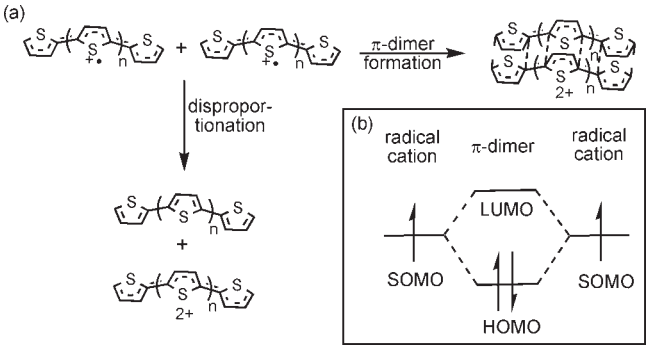

Figure 7. Schematic drawings of (a) π-dimer formation and disproportionation of oligothiophene radical cations and (b) orbital interactions in the formation of a π-dimer.

oxidation states.[20d,21a] This indicates that the methylthio end-capping units played a critical role in stabilizing radical trications.[40] For the generation of tetracations $n\mathbf{P_{Hex}}^{4+}$, the octamer and the decamer required an excess amount of $SbCl_5$, while 9 equivalents of $SbCl_5$ were sufficient to form the tetracation of the dodecamer. At the four-electron oxidation level, the disappearance of the ESR signal was observed again, indicating a singlet character for all of the tetracations. For the dodecamer, even pentacation $\mathbf{12P_{Hex}}^{5+\cdot}$ and hexacation $\mathbf{12P_{Hex}}^{6+}$ were generated, and these states have doublet and singlet characters, respectively, as determined from their spin numbers.

π-Dimer Formation vs Disproportionation. Radical cations of oligothiophenes are the intermediate for the synthesis of polythiophenes via electrochemical and chemical oxidations. However, when persistent radical cations of oligothiohenes can be generated without bulky substituents and with appropriate structural modification to inhibit the radical coupling, the formation of face-to-face dimers (π-dimers) as depicted in Figure 7a can be observed at high concentrations or low temperatures[17−21] as confirmed in the crystal structure of other stable π-radicals.[41−44] From an atoms-in-molecule (AIM) search using the X-ray structure of radical cation π-dimer of a terthiophene end-capped with bicyclo[2.2.2]octene,[24c] it was pointed out that multicenter two-electron bond is formed[45] similar to those seen in the other π-dimers.[41] In general, the absorption bands of a π-dimer in solution are blue-shifted as compared to those of their monomer radicals.[43a] In addition, the bonding SOMO−SOMO interactions of radicals cause a split into the HOMO and the lowest unoccupied molecular orbital (LUMO) of π-dimers (Figure 7b), and a new absorption band corresponding to the HOMO−LUMO transition of the π-dimers is observed in lower energy regions.[43a] Owing to the singlet character of π-dimers that is derived from the bonding between the radical cations (polarons), it was proposed that the π-dimer model can be an alternative to the bipolaron model in highly doped polythiophenes.[17] On the other hand, disproportionation of radical cations (Figure 7a) into neutral and dicationic species is another possible explanation for the singlet character of these species. Although such disproportionation of oligothiophene radical cations has been suggested in the stepwise oxidation process of long oligothioephene,[21] the disproportionation[46] as well as the π-dimer formation[47] is calculated to be an energetically unfavorable process in the gas phase. However, solvation[47] and/or interactions with counteranions[48] would support this process in the condensed phases.

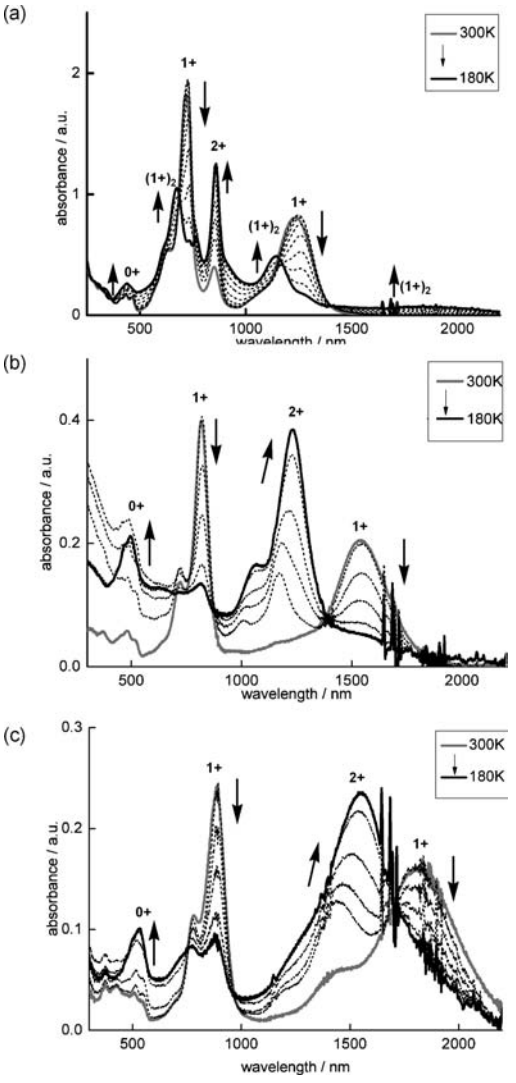

Figure 8. Changes in the absorption spectra upon cooling of the CH_2Cl_2 solutions of (a) $\mathbf{4P_{Hex}}^{+\cdot}$ (233 μM), (b) $\mathbf{6P_{Hex}}^{+\cdot}$ (50.0 μM), and (c) $\mathbf{8P_{Hex}}^{+\cdot}$ (16.6 μM) generated by the reaction of the corresponding neutral species with 1.5 equivalents of $SbCl_5$.

Interestingly, when the absorption spectrum of $\mathbf{4P_{Hex}}^{+\cdot}$ in CH_2Cl_2 was measured at low temperatures, a spectral change corresponding not only to π-dimer formation but also to a disproportionation was observed. As shown in Figure 8a, the reaction of $\mathbf{4P_{Hex}}$ at 233 μM (7 times the concentration than that in Figure 4a) with 1.5 equivalents of $SbCl_5$ gave a mixture of neutral, radical cation, and dication ($\mathbf{4P_{Hex}}$:$\mathbf{4P_{Hex}}^{+\cdot}$:$\mathbf{4P_{Hex}}^{2+}$ = ca. 1:10:1) at room temperature. In general, the equilibrium constant of the disproportionation (K) can be estimated with the equation[49] $K = \exp(-\Delta E_{1/2}F/RT)$, where $\Delta E_{1/2}$ is the difference between first and second oxidation potentials and F the Faraday constant. In the case of $\mathbf{4P_{Hex}}$, the separation of 90 mV (see Table 1) at room temperature predicts K = 0.03, which appears to be in reasonable agreement with the result of the absorption spectra. Upon lowering the temperature, the absorption bands for $\mathbf{4P_{Hex}}^{+\cdot}$ decreased, and new absorption bands (674 nm (1.84 eV), 1145 nm (1.08 eV), ca. 1800 nm (0.69 eV)) appeared in addition to the increase of the absorption bands assigned as $\mathbf{4P_{Hex}}$ and $\mathbf{4P_{Hex}}^{2+}$. These spectral changes were confirmed to be fully reversible.

The new set of absorption bands at low temperatures was considered to be derived from π-dimer $(\mathbf{4P_{Hex}})_2^{2+}$, judging from the similarity of the other oligothiophene radical cation π-dimers.[17−21,24c] Thus, the band in the lower-energy region (~1800 nm) can be assigned as the HOMO−LUMO transition of $(\mathbf{4P_{Hex}})_2^{2+}$. The very broad and weak absorption may indicate that the $\pi-\pi$ interaction was weakened by steric repulsion between the dihexyl side chains in the ProDOT-Hex units. This assumption is consistent with the fact that the π-dimer formation from $\mathbf{4P_{Hex}}^{+\cdot}$ occurs at a much higher concentration than the concentration of $\mathbf{Ph\text{-}3E}^{+\cdot}$ (5 μM) at which the π-dimer formation is observable by using absorption spectra. When the dimerization enthalpy is decreased by steric repulsion, higher concentrations would be necessary for the equilibrium shift to the π-dimer formation.

At 180 K, the absorption band of $\mathbf{4P_{Hex}}^{+\cdot}$ almost disappeared, and the absorption band of $\mathbf{4P_{Hex}}^{2+}$ increased by 3 times, when compared to the spectrum at room temperature. If we assume that $\mathbf{4P_{Hex}}$ was formed in the same amount as $\mathbf{4P_{Hex}}^{2+}$ by the disproportionation and that the rest of $\mathbf{4P_{Hex}}^{+\cdot}$ was used for the formation of $(\mathbf{4P_{Hex}})_2^{2+}$, then the ratio of $\mathbf{4P_{Hex}}$:$\mathbf{4P_{Hex}}^{+\cdot}$:$\mathbf{4P_{Hex}}^{2+}$:$(\mathbf{4P_{Hex}})_2^{2+}$ at 180 K can be roughly estimated to be 3:0:3:3 (= [10 − 2 × (3 − 1)]/2). However, both the π-dimer formation and the disproportionation were found to be sensitive to the initial concentration of $\mathbf{4P_{Hex}}^{+\cdot}$. Thus, the reaction of $\mathbf{4P_{Hex}}$ at 33.2 μM with 1.5 equivalents of $SbCl_5$ mostly gave $\mathbf{4P_{Hex}}^{+\cdot}$ at room temperature, and the equilibrium shift to both the dication and the π-dimer was found to be very small at low temperatures (Figure S4, Supporting Information). If the disproportionation is a simple process, as depicted in Figure 7a, then the equilibrium is not considered to depend on the concentration of the initial radical cation, as the total mole amount of both sides in the disproportionation is the same. Thus, the observed disproportionation may involve unidentified processes, such as self-association of the dication and enhanced interaction between the dication and the counteranions. Regardless, the determination of the thermodynamic parameters is difficult due to the presence of the unidentified process, but the similar concentration- and temperature-dependent spectral changes for both the π-dimer formation and disproportionation suggest that the change in the enthalpy and the entropy for both processes in $\mathbf{4P_{Hex}}^{+\cdot}$ was comparable.

On the other hand, in the case of $\mathbf{6P_{Hex}}^{+\cdot}$ (50.0 μM) and $\mathbf{8P_{Hex}}^{+\cdot}$ (16.6 μM), the equilibrium shift to π-dimer formation was not detected, but the disproportionation was observed at low temperatures (Figure 8b and c), as expected from the negligible difference between first and second oxidation potentials of $\mathbf{6P_{Hex}}$ and $\mathbf{8P_{Hex}}$. These spectral changes were also confirmed to be fully reversible. The absorption band for neutral species appeared at 180 K in the same region as the band that was observed at room temperature, whereas the band for dications at low temperatures showed a gradual bathochromic shift, presumably due to the formation of a *J*-type aggregate of the dications. As another possible process, enhanced interactions between the dication and the counteranions might also take place. However, though such interactions should play an important role in the aggregation of the dication by reducing the electrostatic repulsion between the dications, the interaction itself was not considered to be the reason for the bathochromic shift, as a theoretical study has predicted that such interactions cause rather a hypsochromic shift.[50]

It appeared that $\mathbf{10P_{Hex}}^{+\cdot}$ (16.9 mM) and $\mathbf{12P_{Hex}}^{+\cdot}$ (16.5 μM) also showed only the disproportionation (Figure S4, Supporting Information) at similar concentrations in the same temperature range, although the spectral change was not so clear as that observed in the spectra of $\mathbf{6P_{Hex}}^{+\cdot}$ and $\mathbf{8P_{Hex}}^{+\cdot}$. Thus, the thermodynamic parameters for the disproportionation would be comparable and no apparent oligomer length-dependent change was observed. On the other hand, we also checked the absorption spectra of $\mathbf{10P_{Hex}}^{3+\cdot}$ at low temperatures. However, in this case, spectral changes corresponding to the π-dimer formation or the disproportionation to $\mathbf{10P_{Hex}}^{2+}$ and $\mathbf{10P_{Hex}}^{4+}$ were not observed (Figure S5, Supporting Information). Nevertheless, such disproportionation should take place in the longer oligomer, judging from the mergence of the third and fourth oxidation potentials, as described above, although the detection of such a process in a longer oligomer by using absorption spectra is difficult due to the small spectral change from $\mathbf{12P_{Hex}}^{3+\cdot}$ to $\mathbf{12P_{Hex}}^{4+}$. Overall, these temperature-dependent reversible disproportionation phenomena of oligothiophene radical cations have not yet been reported, and the present study reveals that the disproportionation is more favorable than π-dimer formation for $n\mathbf{P_{Hex}}^{+\cdot}$. In this context, π-dimer formation is not necessarily essential for the singlet character of highly doped poly(3,4-alkylenedioxythiophene).

Table 3. Relative Energies for $n\mathbf{P_H}^{2+}$ and $n\mathbf{T}^{2+}$ in Spin-Restricted Singlet (R), Spin-Unrestricted Singlet (U), and Triplet (T) States at the B3LYP/6-31G(d) Level and S^2 Values and Biradical Indices of the Singlet Biradical (U) States

compd	$\Delta E_{(R-U)}$ [a]	$\Delta E_{(T-U)}$ [a]	$\Delta E_{(T-R)}$ [a]	$\langle S^2 \rangle$ [b]	biradical index [c]
$\mathbf{6P_H}^{2+}$	0.04	5.62	5.59	0.17	8%
$\mathbf{8P_H}^{2+}$	0.95	2.78	1.83	0.68	40%
$\mathbf{10P_H}^{2+}$	1.97	1.61	−0.35	0.85	55%
$\mathbf{12P_H}^{2+}$	3.10	0.85	−2.26	0.94	67%
$\mathbf{6T}^{2+}$	0.2 [d]	6.0 [d]	5.8 [d]	0.32 [d]	16%
$\mathbf{8T}^{2+}$	1.6 [d]	2.7 [d]	1.1 [d]	0.77 [d]	47%
$\mathbf{10T}^{2+}$	3.2 [d]	1.3 [d]	−1.8 [d]	0.92 [d]	62%
$\mathbf{12T}^{2+}$	4.2 [d]	0.7 [d]	−3.5 [d]	0.98 [d]	72%

[a] The data are given in kcal/mol. [b] Before annihilation. [c] Estimated by natural orbital occupation number (NOON) analysis at the B3LYP/6-31G(d) level. [d] Ref 46.

Bipolaron vs Polaron Pair. The other possible reason for the singlet character of highly p-doped polythiophenes is a singlet polaron pair (singlet biradical dication), and it has been studied mainly by theoretical calculations. In recent studies, the broken symmetry method has been used to predict the electronic structure of the singlet biradical dication of oligothiophenes as a polaron pair model,[34,46,48,50,51] and the singlet polaron pair has been shown to be the ground state for long oligothiophene dications.[46] To predict the effect of the dioxy substituents on the biradical character of oligothiophene dications, we performed DFT calculations (B3LYP/6-31G(d)) of ProDOT oligomer dication $n\mathbf{P_H}^{2+}$ with methylthio end-capping groups, and the results were compared with unsubstituted oligothiophene dication $n\mathbf{T}^{2+}$.[46]

In the case of $n\mathbf{T}^{2+}$, the energy of the spin-unrestricted (U) wave function (UB3LYP/6-31G(d)) for the open-shell singlet configuration (singlet biradical) was reported to become lower than that of spin-restricted (R) wave function (RB3LYP/6-31G(d)) of the closed-shell configuration when $n > 6$.[46,51,52] In the same oligomer length, the singlet biradical state (U) of $n\mathbf{P_H}^{2+}$ became lower in energy than the closed-shell singlet state (R). As shown in Table 3, the energy differences ($\Delta E_{(R-U)} = E_{(RB3LYP)} - E_{(UB3LYP)}$) in $n\mathbf{P_H}^{2+}$ (0.04, 0.95, 2.0, and 3.1) increased with increasing chain length. However, they were slightly lower than those of $n\mathbf{T}^{2+}$ (0.2, 1.6, 3.2, and 4.2 kcal mol^{-1}, respectively). Taking into consideration that the methylthio end-capping was shown to slightly stabilize the

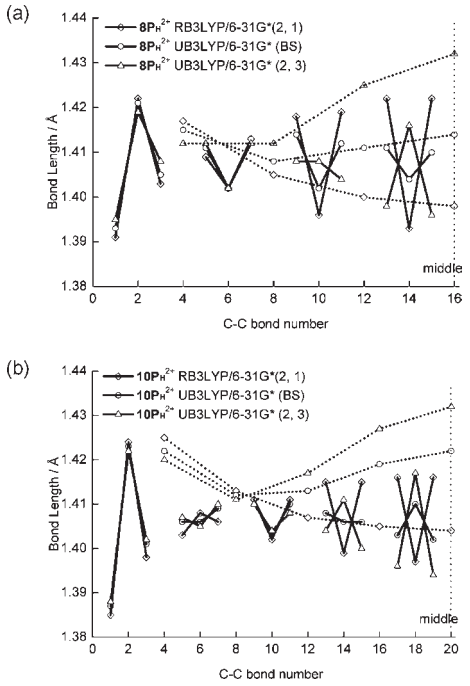

Figure 9. BLA for (a) $\mathbf{8P_H}^{2+}$ and (d) $\mathbf{10P_H}^{2+}$ with C_i symmetry. The x-axis is the C−C bond number starting from one end of the conjugated chain through to the middle of that chain. The repeating sets of three linked points correspond to intraring bonds, while every fourth point on the x-axis indicates an inter-ring C−C bond.

singlet biradical state,[26] the slightly lower $\Delta E_{(R\text{-}U)}$ for $n\mathbf{P_H}^{2+}$ as compared to $n\mathbf{T}^{2+}$ indicates that the dioxy substituents stabilized closed-shell states or destabilized the singlet biradical states to at least some extent.

The energy differences between the triplet (T) and singlet biradical (U) states ($\Delta E_{(T-U)}$) of $n\mathbf{P_H}^{2+}$ were also positive. Hence, the singlet biradical state was the lowest in energy between the oligomer lengths, where $6 \leq n \leq 12$. On the other hand, the $\Delta E_{(T-U)}$ of $n\mathbf{P_H}^{2+}$ decreased with increasing chain length, and consequently, the sign of $\Delta E_{(T-R)}$ was shown to change from positive to negative at approximately the decamer length. Thus, the triplet state is predicted to be more stable than the closed-shell singlet state in the longer oligomers. As a result, in the optimized structures of $n\mathbf{P_H}^{2+}$, the pattern of carbon−carbon bond length alternation (BLA) of the singlet biradical states in the case of $n \geq 10$ becomes more similar to that of triplet states rather than that of closed-shell singlet states. As shown in Figure 9, the structural difference between open- and closed-shell states appears especially in the central thiophene rings, where the singlet biradical state of $\mathbf{10P_H}^{2+}$ and the triplet state have an "aromatic" BLA pattern (a Λ-shaped pattern in the sets of the three linked data points)[46,53] in contrast to a quinoid BLA pattern (a V-shaped pattern in the sets of three linked data points) for the singlet biradical state of $\mathbf{8P_H}^{2+}$ and the closed-shell singlet states. These results are rationalized by the hypothesis that a radical cation pair tends to separate in the longer oligomer dication. Similar chain length dependence of $\Delta E_{(T-U)}$ and $\Delta E_{(T-R)}$ and structural changes was also observed for $n\mathbf{T}^{2+}$. Therefore, the biradical character of $n\mathbf{P_H}^{2+}$ and $n\mathbf{T}^{2+}$ would start to emerge at similar chain lengths.

Concerning the electronic structure of the singlet biradicals (U), the spin distributions of $n\mathbf{P_H}^{2+}$ (Figure S6, Supporting Information) were delocalized over the whole π-system. The S^2 values of the singlet biradical states of $n\mathbf{P_H}^{2+}$ increased with increasing chain length as observed for $n\mathbf{T}^{2+}$[46], and the values of $n\mathbf{P_H}^{2+}$ (0.17−0.94) were slightly lower than those of $n\mathbf{T}^{2+}$ within the same chain length (Table 3). The biradical indices of $n\mathbf{P_H}^{2+}$ (n = 6, 8, 10, and 12) estimated by natural orbital occupation number (NOON) analysis[54] at the B3LYP/6-31G(d) level (8−67%) were also slightly lower than those of $n\mathbf{T}^{2+}$ with the same chain length. Thus, the dioxy substituents were shown to slightly reduce the biradical character of oligothiophene dications.

Next, the absorption band and oscillator strength of $n\mathbf{P_H}^{2+}$ were calculated by the TD-DFT method at the B3LYP/6-31G(d) level, and the results were compared with the observed absorption spectra of $n\mathbf{P_{Hex}}^{2+}$. Because $n\mathbf{P_{Hex}}^{2+}$ was observed to be almost ESR inactive, the results of the closed-shell singlet (R) and singlet biradical (U) states were compared. As shown in Table 4, the calculated closed-shell (R) state mainly involves one strong absorption band assigned as the HOMO−LUMO transition, and the oscillator strength increased with increasing chain length. However, the observed absorption coefficient (Table 2) decreased from $\mathbf{8P_{Hex}}^{2+}$ to $\mathbf{10P_{Hex}}^{2+}$. In addition, the absorption band for $\mathbf{10P_{Hex}}^{2+}$ broadened accompanied by weak absorption bands at approximately 1.5−2 eV (620−830 nm), as shown in Figure 10. These results are similar to the previous observations seen in the absorption spectra of

Table 4. Excitation Energies (E_{calc}) and Oscillator Strengths (f) of $n\mathbf{P_H}^{2+}$ in Spin-Restricted (R) and Spin-Unrestricted (U) Singlet States Calculated by the TD-B3LYP/6-31G(d) Method[a]

compd	state	$E_{calc}{}^{1\,b}$	$E_{calc}{}^{2\,b}$	$E_{calc}{}^{3\,b}$	$E_{calc}{}^{4\,b}$
$\mathbf{6P_H}^{2+}$	R	1.37 (3.06)	–	–	–
	U	1.35 (3.05)	–	–	–
$\mathbf{8P_H}^{2+}$	R	1.09 (3.97)	–	–	–
	U	0.95 (1.81)	1.08 (0.89)	1.62 (1.27)	–
$\mathbf{10P_H}^{2+}$	R	0.90 (4.55)	2.08 (0.46)	–	–
	U	0.67 (2.70)	0.86 (0.16)	1.27 (0.21)	1.47 (1.66)
$\mathbf{12P_H}^{2+}$	R	0.73 (4.88)	1.88 (0.13)	1.90 (0.92)	–
	U	0.67 (2.98)	1.47 (2.30)	1.56 (0.42)	–

[a] Excitation energies from 10 exited states are selected with an oscillator strength (f) of more than 0.1. [b] The calculated absorption bands are given in eV with oscillator strengths (f) in parentheses.

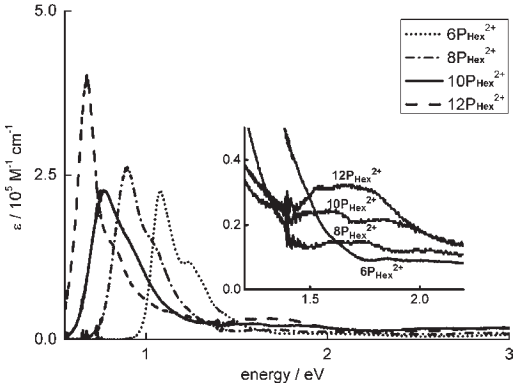

Figure 10. Comparison of the absorption spectra of $n\mathbf{P_{Hex}}^{2+}$. Insets are enlargements of the region for the second absorption bands of the dications.

oligothiophene dications annelated with bicyclo[2.2.2]octene units.[24d] In these cases, the observed results were in reasonable agreement with the calculated spectra of the singlet biradical at the TDB3P86-30% level.[50] Thus, it seems that the biradical character starts to appear at approximately $n = 10$ for $n\mathbf{P}_{\mathbf{Hex}}^{2+}$. However, the TD-B3LYP/6-31G(d) method predicted that singlet biradical (U) states of $\mathbf{10P}_{\mathbf{Hex}}^{2+}$ and $\mathbf{12P}_{\mathbf{Hex}}^{2+}$ involve two absorptions and that the oscillator strength for the second band is much stronger than that of observed one. On the other hand, the absorption spectra of the singlet biradical state of dication of thiophene-pyrrole mixed oligomers were well reproduced by the TD-B3LYP/6-31G(d) method, only when the biradical index was high (71% at B3LYP/6-31G(d) for oligomers composed of seven thiophene, two pyrrole, and methylthio end-capping units).[26] In this context, the discrepancy between the observed spectra for $\mathbf{10P}_{\mathbf{Hex}}^{2+}$ and $\mathbf{12P}_{\mathbf{Hex}}^{2+}$ and the calculated spectra for $\mathbf{10P}_{\mathbf{H}}^{2+}$ and $\mathbf{12P}_{\mathbf{H}}^{2+}$ would be due to the lower biradical character of these oligomers.

To investigate the closed- or open-shell nature of the oligomer dication, the ^{1}H NMR spectra of $n\mathbf{P}_{\mathbf{Hex}}^{2+}$ that was generated with 3 equivalents of $SbCl_5$ in CD_2Cl_2 were collected. As expected, the ^{1}H NMR signals of $\mathbf{6P}_{\mathbf{Hex}}^{2+}$ were observed: one was collected at 210 K and the other at room temperature in the presence of $Fe(C_5H_4Ac)_2 \cdot AgBF_4$ for reducing radical impurity[55] (Figure S7, Supporting Information). The chemical shift for the methyleneoxy and methylthio protons showed downfield shifts by approximately 0.5 ppm upon the two-electron oxidation. This result clearly indicates the closed-shell nature of $\mathbf{6P}_{\mathbf{Hex}}^{2+}$. However, ^{1}H NMR signals of the longer oligomer dications ($\mathbf{8P}_{\mathbf{Hex}}^{2+}$, $\mathbf{10P}_{\mathbf{Hex}}^{2+}$, and $\mathbf{12P}_{\mathbf{Hex}}^{2+}$ (Figure S8, Supporting Information) showed severe broadening. These results support the open-shell nature of longer oligomer dications.[56] On the other hand, the ^{1}H NMR spectrum of $\mathbf{10P}_{\mathbf{Hex}}^{4+}$ (Figure S9, Supporting Information) that was generated with an excess $SbCl_5$ in CD_2Cl_2 showed signals that were 0.8−1 ppm downfield in comparison with those of neutral $\mathbf{10P}_{\mathbf{Hex}}$. From these results, PProDOT with high doping levels of more than approximately 25% has a closed-shell structure (i.e., bipolaron), whereas less than approximately 20% doping level is considered to show an open-shell structure (i.e., polaron pair).

Comparison with PEDOT in the p-Doped States. Because $n\mathbf{P}_{\mathbf{Hex}}$ showed similar structural and electronic properties to EDOT oligomers in the neutral state, both the ProDOT and EDOT polymers in the p-doped states should also share common features. Thus, from the results of the present study, the following conclusions can be drawn for the p-doped states of poly(3,4-alkylenedioxythiophene)s: (1) The oxidation potentials are lowered by the electron-donating dioxy substituents, which enable up to an approximate 60% doping level (six-electron oxidation of $\mathbf{10P}_{\mathbf{Hex}}$) below 1.0 V vs Fc/Fc^+ (ca. 1.5 V vs SCE); (2) in the single chain with less than an approximate 40% doping level, p-doped states with an even number of electrons are more favorable than those with an odd number of electrons (judging from the mergence of the third and fourth oxidation potentials of $\mathbf{10P}_{\mathbf{Hex}}$); (3) disproportionation is as important or more important than π-dimer formation for the spinless character in the high p-doping level; (4) the dioxy substituents slightly weaken the biradical character derived from the transition from bipolaron to polaron pair, and the biradical character starts to appear at less than an approximate 20% doping level (judging from the biradical character of $\mathbf{10P}_{\mathbf{Hex}}^{2+}$); and (5) electronic absorption in visible region is mainly due to polaron or its interchain pair (π-dimer), and the absorption band for the bipolaron appears mostly in the NIR region. As for (2), this conclusion would be attributable to the quinoidal resonance structures, such as those shown in Scheme 2, where the electron-donating dioxy substituents play an important role. As a result, the disproportionation described in (3) is considered to be facilitated, owing to the favorable state described in (2).

Scheme 2. Plausible Resonance Structures of Poly(3,4-alkylenedioxythiophene) at the 40% p-Doping Level

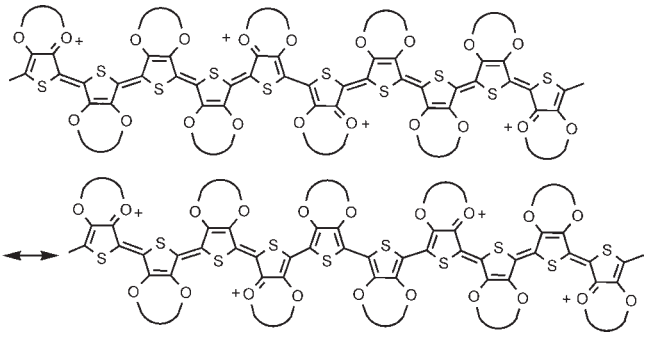

For electrochemically prepared alkylated-PEDOT, high conductivity (200−850 S/cm) holds during the high doping level of between an approximate 30% and 60%, where no absorption band was observed in the visible region. From the results of in situ ESR, it was concluded that bipolaron is responsible for the high conductivity.[57] These facts are consistent with the conclusions derived in the present study. In this context, a weak absorption band at approximately 900 nm observed in the PEDOT-PSS films would be assigned as not a "bipolaron subgap transition"[58] but due to a polaron (or its interchain pair (π-dimer)). On the other hand, polythiophenes with alkyl side chains in high p-doping levels usually show two absorption bands in the NIR region (~2500 nm) and visible region (~800 nm),[20d,35,36] which should involve the polaron[59] (or intra- and interchain polaron pairs). Overall, the dioxy substituents in poly(3,4-alkylenedioxythiophene)s, which can stabilize the high p-doping levels with the closed-shell bipolaron structure owing to their electron-donating properties, play a critical role in the high conductivity and transparency properties of the polymer.

CONCLUSION

We have synthesized new ProDOT oligomers end-capped with methylthio groups ($n\mathbf{P}_{\mathbf{Hex}}$) up to the dodecamer length, and we succeeded in the first systematic study on the structural, optical, and electronic properties of a series of ProDOT oligomers in neutral and various oxidation states. From the comparison of the properties of $n\mathbf{P}_{\mathbf{Hex}}$ in the neutral state with those of the EDOT oligomers, ProDOT oligomers were found to serve as a model of not only PProDOT but also PEDOT. From the measurements of $n\mathbf{P}_{\mathbf{Hex}}$ in various oxidation states by means of CV, UV−vis−NIR, ESR, and NMR techniques, together with theoretical calculations, we revealed that the electron-donating dioxy substituents in EDOT and ProDOT stabilized a closed-shell bipolaron structure in high p-doping levels, which enable the high conductivity and transparency properties of the 3,4-alkylenedioxythiophene polymers. The detailed understanding of the optical and electronic properties of 3,4-alkylenedioxythiophene oligomers provided by the present study will guide the rational design of other transparent conductive polythiophenes and related polymers, which are important classes of materials in the development of rare metal-free transparent electrodes.

■ ASSOCIATED CONTENT

Supporting Information. Experimental procedures and the characterization data of **2**−**11** and $n\mathbf{P}_{\mathbf{Hex}}$ (n = 4,6,8,10, and12); Figures S1−S9; Cartesian coordinates and total energies of the optimized structures of all calculated molecules (B3LYP/6-31G(d)); and crystallographic information files (CIF) for **11**. This material is available free of charge via the Internet at http://pubs.acs.org

■ AUTHOR INFORMATION

Corresponding Author
nishinaga-tohru@tmu.ac.jp

■ ACKNOWLEDGMENT

This work was supported by a Grant-in-Aid for Scientific Research (no. 22350021).

■ REFERENCES

(1) For reviews, see: (a) Kirchmeyer, S.; Reuter, K. *J. Mater. Chem.* **2005**, *15*, 2077–2088. (b) Groenendaal, L.; Zotti, G.; Aubert, P. H.; Waybright, S. M.; Reynolds, J. R. *Adv. Mater.* **2003**, *15*, 855–879. (c) Groenendaal, L.; Jonas, F.; Freitag, D.; Pielartzik, H.; Reynolds, J. R. *Adv. Mater.* **2000**, *12*, 481–494.

(2) (a) Beaujuge, P. M.; Amb, C. M.; Reynolds, J. R. *Acc. Chem. Res.* **2010**, *43*, 1396–1407. (b) Beaujuge, P. M.; Reynolds, J. R. *Chem. Rev.* **2010**, *110*, 268–320.

(3) (a) Heywang, G.; Jonas, F. *Adv. Mater.* **1992**, *4*, 116–118. (b) Dietrich, M.; Heize, J.; Heywang, G.; Jonas, F. *J. Electroanal. Chem.* **1994**, *369*, 87–92.

(4) (a) Kumar, A.; Welsh, D. M.; Morvant, M. C.; Piroux, F.; Abboud, K. A.; Reynolds, J. R. *Chem. Mater.* **1998**, *10*, 896–902. (b) Groenendaal, L.; Jonas, F.; Freitag, D.; Pielartzik, H.; Reynolds, J. R. *Adv. Mater.* **2000**, *12*, 481–494. (c) Welsh, D. M.; Kloeppner, L. J.; Madrigal, L.; Pinto, M. R.; Thompson, B. C.; Schanze, K. S.; Abboud, K. A.; Powell, D.; Reynolds, J. R. *Macromolecules* **2002**, *35*, 6517–6525. (d) Cirpan, A.; Argun, A. A.; Grenier, C. R. G.; Reeves, B. D.; Reynolds, J. R. *J. Mater. Chem.* **2003**, *13*, 2422–2428. (e) Reeves, B. D.; Grenier, C. R. G.; Argun, A. A.; Cirpan, A.; McCarley, T. D.; Reynolds, J. R. *Macromolecules* **2004**, *37*, 7559–7569. (f) Mishra, S. P.; Sahoo, R.; Ambade, A. V.; Contractor, A. Q.; Kumar, A. *J. Mater. Chem.* **2004**, *14*, 1896–1900. (g) Reeves, B. D.; Unur, E.; Ananthakrishnan, N.; Reynolds, J. R. *Macromolecules* **2007**, *40*, 5344–5352. (h) Grenier, C. R. G.; George, S. J.; Joncheray, T. J.; Meijer, E. W.; Reynolds, J. R. *J. Am. Chem. Soc.* **2007**, *129*, 10694–10699. (i) Sinha, J.; Sahoo, R.; Kumar, A. *Macromolecules* **2009**, *42*, 2015–2022.

(5) Nielsen, C. B.; Bjørnholm, T. *Macromolecules* **2005**, *38*, 10379–10387.

(6) Müllen, K.; Wegner, G. *Electronic Materials: The Oligomer Approach*, Wiley: Chichester, U.K., 1998.

(7) (a) Sotzing, G. A.; Reynolds, J. R.; Steel, P. J. *Chem. Mater.* **1996**, *8*, 882–889. (b) Sotzing, G. A.; Reynolds, J. R.; Steel, P. J. *Adv. Mater.* **1997**, *9*, 795–798. (c) Zhu, S. S.; Swager, T. M. *J. Am. Chem. Soc.* **1997**, *119*, 12568–12577. (d) Akoudad, S.; Roncali, J. *Synth. Met.* **1998**, *93*, 111–114.

(8) Hicks, R. G.; Nodwell, M. B. *J. Am. Chem. Soc.* **2000**, *122*, 6746–6753.

(9) Apperloo, J. J.; Groenendaal, L. B.; Verheyen, H.; Jayakannan, M.; Janssen, R. A. J.; Dkhissi, A.; Beljonne, D.; Lazzaroni, R.; Brédas, J. L. *Chem.—Eur. J.* **2002**, *8*, 2384–2396.

(10) De Jong, M. P.; van der Gon, A. W. D.; Crispin, X.; Osikowicz, W.; Salaneck, W. R.; Groenendaal, L. *J. Chem. Phys.* **2003**, *118*, 6495–6502.

(11) Turbiez, M.; Frère, P.; Roncali, J. *J. Org. Chem.* **2003**, *68*, 5357–5360.

(12) Wasserberg, D.; Meskers, S. C. J.; Janssen, R. A. J.; Mena-Osteritz, E.; Bäuerle, P. *J. Am. Chem. Soc.* **2006**, *128*, 17007–17017.

(13) (a) Nielsen, C. B.; Angerhofer, A.; Abboud, K. A.; Reynolds, J. R. *J. Am. Chem. Soc.* **2008**, *130*, 9734–9746. (b) Hammond, S. R.; Clot, O.; Firestone, K. A.; Bale, D. H.; Lao, D.; Haller, M.; Phelan, G. D.; Carlson, B.; Jen, A. K.-Y.; Reid, P. J.; Dalton, L. R. *Chem. Mater.* **2008**, *20*, 3425–3434. (c) Liang, Y.; Peng, B.; Liang, J.; Tao, Z.; Chen, J. *Org. Lett.* **2010**, *12*, 1204–1207.

(14) (a) Otsubo, T.; Aso, Y.; Takimiya, K. *Bull. Chem. Soc. Jpn.* **2001**, *74*, 1789–1801. (b) Fichou, D. *Handbook of Oligo- and Polythiophenes*; Wiley-VCH: Weinheim, Germany, 1999. (c) Miller, L. L.; Mann, K. R. *Acc. Chem. Res.* **1996**, *29*, 417–423.

(15) (a) Fichou, D.; Xu, B.; Horowitz, G.; Garnier, F. *Synth. Met.* **1991**, *41*, 463–469. (b) Nessakh, B.; Horowitz, G.; Garnier, F.; Deloffre, F.; Srivastava, P.; Yassar, A. *J. Electroanal. Chem.* **1995**, *399*, 97–103.

(16) Caspar, J. V.; Ramamurthy, V.; Corbin, D. R. *J. Am. Chem. Soc.* **1991**, *113*, 600–610.

(17) (a) Hill, M. G.; Penneau, J.-F.; Zinger, B.; Mann, K. R.; Miller, L. L. *Chem. Mater.* **1992**, *4*, 1106–1113. (b) Hill, M. G.; Mann, K. R.; Miller, L. L.; Penneau, J.-F. *J. Am. Chem. Soc.* **1992**, *114*, 2728–2730. (c) Yu, Y.; Gunic, E.; Zinger, B.; Miller, L. L. *J. Am. Chem. Soc.* **1996**, *118*, 1013–1018. (d) Graf, D. D.; Duan, R. G.; Campbell, J. P.; Miller, L. L.; Mann, K. R. *J. Am. Chem. Soc.* **1997**, *119*, 5888–5899.

(18) Guay, J.; Kasai, P.; Diaz, A.; Wu, R.; Tour, J. M.; Dao, L. H. *Chem. Mater.* **1992**, *4*, 1097–1105.

(19) (a) Bäuerle, P.; Segelbacher, U.; Maier, A.; Mehring, M. *J. Am. Chem. Soc.* **1993**, *115*, 10217–10223. (b) Bäuerle, P.; Fischer, T.; Bidlingmeier, B.; Rabe, J. P.; Stabel, A. *Angew. Chem., Int. Ed. Engl.* **1995**, *34*, 303–307. (c) Zhang, F.; Götz, G.; Mena-Osteritz, E.; Weil, M.; Sarkar, B.; Kaim, W.; Bäuerle, P. *Chem. Sci.* **2011**, *2*, 781–784.

(20) (a) Nakanishi, H.; Sumi, N.; Aso, Y.; Otsubo, T. *J. Org. Chem.* **1998**, *63*, 8632–8633. (b) Nakanishi, H.; Sumi, N.; Ueno, S.; Takimiya, K.; Aso, Y.; Otsubo, T.; Komaguchi, K.; Shiotani, M.; Ohta, N. *Synth. Met.* **2001**, *119*, 413–414. (c) Sakai, T.; Satou, T.; Kaikawa, T.; Takimiya, K.; Otsubo, T.; Aso, Y. *J. Am. Chem. Soc.* **2005**, *127*, 8082–8089. (d) Kurata, T.; Mohri, T.; Takimiya, K.; Otsubo, T. *Bull. Chem. Soc. Jpn.* **2007**, *80*, 1799–1807. (e) Casado, J.; Takimiya, K.; Otsubo, T.; Ramírez, F. J.; Quirante, J. J.; Ortiz, R. P.; González, S. R.; Oliva, M. M.; Navarrete, J. T. L. *J. Am. Chem. Soc.* **2008**, *130*, 14028–14029. (f) Ie, Y.; Han, A.; Otsubo, T.; Aso, Y. *Chem. Commun.* **2009**, 3020–3022.

(21) (a) van Haare, J. A. E. H.; Havinga, E. E.; van Dongen, J. L. J.; Janssen, R. A. J.; Cornil, J.; Brédas, J.-L. *Chem.—Eur. J.* **1998**, *4*, 1509–1522. (b) Apperloo, J. J.; Janssen, R. A. J.; Malenfant, P. R. L.; Groenendaal, L.; Fréchet, J. M. J. *J. Am. Chem. Soc.* **2000**, *122*, 7042–7051.

(22) Rohde, D.; Dunsch, L.; Tabet, A.; Hartmann, H.; Fabian, J. *J. Phys. Chem. B* **2006**, *110*, 8223–8231.

(23) Haubner, K.; Tarábek, J.; Ziegs, F.; Lukeš, V.; Jaehne, E.; Dunsch, L. *J. Phys. Chem. A* **2010**, *114*, 11545–11551.

(24) (a) Wakamiya, A.; Yamazaki, D.; Nishinaga, T.; Kitagawa, T.; Komatsu, K. *J. Org. Chem.* **2003**, *68*, 8305–8314. (b) Nishinaga, T.; Wakamiya, A.; Yamazaki, D.; Komatsu, K. *J. Am. Chem. Soc.* **2004**, *126*, 3163–3174. (c) Yamazaki, D.; Nishinaga, T.; Tanino, N.; Komatsu, K. *J. Am. Chem. Soc.* **2006**, *128*, 14470–14471. (d) Nishinaga, T.; Yamazaki, D.; Tateno, M.; Iyoda, M.; Komatsu, K. *Materials* **2010**, *3*, 2037–2052.

(25) (a) Nishinaga, T.; Komatsu, K. *Org. Biomol. Chem.* **2005**, *3*, 561–569. (b) Komatsu, K.; Nishinaga, T. *Synlett* **2005**, 187–202.

(26) Nishinaga, T.; Tateno, M.; Fujii, M.; Fujita, W.; Takase, M.; Iyoda, M. *Org. Lett.* **2010**, *12*, 5374–5377.

(27) (a) Roncali, J.; Blanchard, P.; Frère, P. *J. Mater. Chem.* **2005**, *15*, 1589–1610. (b) Raimundo, J.-M.; Blanchard, P.; Frère, P.; Mercier, N.; Ledoux-Rak, I.; Hierle, R.; Roncali, J. *Tetrahedron Lett.* **2001**, *42*, 1507–1510. (c) Turbiez, M.; Frère, P.; Allain, M.; Videlot, C.; Ackerman, J.; Roncali, J. *Chem.—Eur. J.* **2005**, *11*, 3742–3752.

(28) Poater, J.; Casanovas, J.; Solà, M.; Alemán, C. *J. Phys Chem. A* **2010**, *114*, 1023–1028.

(29) Bidan, G.; De Nicola, A.; Enée, V.; Guillerez, S. *Chem. Mater.* **1998**, *10*, 1052–1058.

(30) Izumi, T.; Kobashi, S.; Takimiya, K.; Aso, Y.; Otsubo, T. *J. Am. Chem. Soc.* **2003**, *125*, 5286–5287.

(31) (a) Zade, S. S.; Zamoshchik, N.; Bendikov, M. *Acc. Chem. Res.* **2011**, *44*, 14–24. (b) Zade, S. S.; Bendikov, M. *Org. Lett.* **2006**, *8*, 5243–5246.
(32) Casado, J.; Zgierski, M. Z.; Hicks, R. G.; Myles, D. J. T.; Viruela, P. M.; Ortí, E.; Delgado, M. C. R.; Hernández, V.; Navarrete, J. T. L. *J. Phys. Chem. A* **2005**, *109*, 11275–11284.
(33) Otani, T.; Hachiya, M.; Hashizume, D.; Matsuo, T.; Tamao, K. *Chem. Asian J.* **2011**, *6*, 350–354.
(34) Zade, S. S.; Bendikov, M. *J. Phys. Chem. C* **2007**, *111*, 10662–10672 In the case of $\mathbf{10T}^{3+}$, the energy difference is 8.4 kcal mol^{-1} at the B3LYP/6-31G(d) level.
(35) Kaneto, K.; Hayashi, S.; Ura, S.; Yoshino, K. *J. Phys. Soc. Jpn.* **1985**, *54*, 1146–1153.
(36) Chen, J.; Heeger, A. J.; Wudl, F. *Solid. State Commun.* **1986**, *58*, 251–257.
(37) Brédas, J. L.; Street, G. B. *Acc. Chem. Res.* **1985**, *18*, 309–315.
(38) Smie, A.; Heinze, J. *Angew. Chem., Int. Ed. Engl.* **1997**, *36*, 363–367.
(39) (a) Takahashi, T.; Matsuoka, K.; Takimiya, K.; Otsubo, T.; Aso, Y. *J. Am. Chem. Soc.* **2005**, *127*, 8928–8929. (b) Ortiz, R. P.; Casado, J.; Hernández, V.; Navarrete, J. T. L.; Viruela, P. M.; Ortí, E.; Takimiya, K.; Otsubo, T. *Angew. Chem., Int. Ed.* **2007**, *46*, 9057–9061.
(40) The relatively small spin number for trications of longer oligomers ($n \geq 8$) may be due to mixing with tetracation.
(41) (a) Miller, J. S.; Novoa, J. J. *Acc. Chem. Res.* **2007**, *40*, 189–196. (b) Novoa, J. J.; Lafuente, P.; Del Sesto, R. E.; Miller, J. S. *Angew. Chem., Int. Ed.* **2001**, *40*, 2540–2545. (c) Del Sesto, R. E.; Miller, J. S.; Novoa, J. J.; Lafuente, P. *Chem.—Eur. J.* **2002**, *8*, 4894–4908. (d) Mota, F.; Miller, J. S.; Novoa, J. J. *J. Am. Chem. Soc.* **2009**, *131*, 7699–7707. (e) Novoa, J. J.; Stephens, P. W.; Weerasekare, M.; Shum, W. W.; Miller, J. S. *J. Am. Chem. Soc.* **2009**, *131*, 9070–9075.
(42) Goto, K.; Kubo, T.; Yamamoto, K.; Nakasuji, K.; Sato, K.; Shiomi, D.; Takui, T.; Kubota, M.; Kobayashi, T.; Yakusi, K.; Ouyang, J. *J. Am. Chem. Soc.* **1999**, *121*, 1619–1620.
(43) (a) Lü, J.-M.; Rosokha, S. V.; Kochi, J. K. *J. Am. Chem. Soc.* **2003**, *125*, 12161–12171. (b) Rosokha, S. V.; Lu, J.; Han, B.; Kochi, J. K. *New J. Chem.* **2009**, *33*, 545–553.
(44) Shuvaev, K. V.; Decken, A.; Grein, F.; Abedin, T. S. M.; Thompson, L. K.; Passmore, J. *Dalton Trans.* **2008**, 4029–4037.
(45) Yoldi, I. G.; Miller, J. S.; Novoa, J. J. *Theor. Chem. Acc.* **2009**, *123*, 137–143.
(46) Zade, S. S.; Bendikov, M. *J. Phys. Chem. B* **2006**, *110*, 15839–15846.
(47) Scherlis, D. A.; Marzari, N. *J. Phys. Chem. B* **2004**, *108*, 17791–17795.
(48) Zamoshchik, N.; Salzner, U.; Bendikov, M. *J. Phys. Chem. C* **2008**, *112*, 8408–8418.
(49) Richardson, E.; Taube, H. *Inorg. Chem.* **1981**, *20*, 1278–1285.
(50) Salzner, U. *J. Phys. Chem. A* **2008**, *112*, 5458–5466.
(51) Gao, Y.; Liu, C.-G.; Jiang, Y.-S. *J. Phys. Chem. A* **2002**, *106*, 5380–5384.
(52) The oligomer length at which open-shell singlet ground state of $n\mathbf{T}^{2+}$ starts is highly dependent on the method of calculations. UB3P86-30% calculations predicted that it starts at $n = 4$ (see ref 50), while UBLYP calculations showed it starts at $n = 20$ (see ref 46).
(53) Geskin, V. M.; Brédas, J.-L. *Chem. Phys. Chem.* **2003**, *4*, 498–505.
(54) Döhnert, D.; Koutecký, J. *J. Am. Chem. Soc.* **1980**, *102*, 1789–1796.
(55) Zheng, S.; Barlow, S.; Risko, C.; Kinnibrugh, T. L.; Timofeeva, T. V.; Coropceanu, V.; Brédas, J.-L.; Marder, S. R. *J. Am. Chem. Soc.* **2006**, *128*, 1812–1817.
(56) The contamination with radical cation or radical trication which causes the broadening of the signal by rapid exchange with dication cannot be ruled out.
(57) Groenendaal, L.; Zotti, G.; Jonas, F. *Synth. Met.* **2001**, *118*, 105–109.
(58) Ouyang, J.; Xu, Q.; Chu, C.-W.; Yang, Y.; Li, C.; Shinar, J. *Polymer* **2004**, *45*, 8443–8450.
(59) Furukawa, Y. *J. Phys. Chem.* **1996**, *100*, 15644–15653.